Discharge-modulated soil organic carbon export from temperate mountainous headwater streams

Hannah Gies[1], Maarten Lupker[1], Silvan Wick[2], Negar Haghipour[1,3], Björn Buggle[4], Timothy Eglinton[1]

[1]Geological Institute, Department of Earth Sciences, ETH Zürich, Zürich, Switzerland
[2]Soil Science and Biogeochemistry, Department of Geography, University of Zürich, Zürich, Switzerland
[3]Laboratory of Ion Beam Physics, Department of Physics, ETH Zürich, Zürich,Switzerland
[4]Dorfstraße 10, Wennigsen, Germany

Key Points:

- the composition of suspended sediment is variable at low discharges, but converges towards a defined endmember mixture as runoff increases
- soil organic carbon export increases with discharge at a similar rate in all studied catchments indicating common mobilization processes
- runoff-driven soil erosion in the studied rivers is responsible for the export of ca. 0.3 to 0.8 gC m^{-2} a^{-1} as particulate organic carbon

Corresponding author: Hannah Gies, hannah.gies@erdw.ethz.ch

Abstract

Erosion and riverine transport of organic carbon is an important component of the global carbon cycle, but the significance of this process for Earth's surface carbon budgets depends on the sources of carbon being mobilised. In this study, we aim to constrain how runoff-driven erosion modulates the contribution of different carbon source endmembers, i.e., bedrock, soil and vegetation, in three forested headwater catchments in the Swiss Prealps. The sources of organic carbon are determined using an inverse model based on bulk carbon isotope signatures and the abundances and distributions of long-chain n-alkane plant wax biomarkers in suspended sediments collected over a range of discharges. Despite landcover differences and contrasting bulk particulate organic carbon (POC) signatures, the increase of soil-sourced organic carbon with discharge is similar in all three studied catchments. This apparent existence of common processes implies that export fluxes of soil organic carbon may be extrapolated to similar catchments. Overall, our analysis shows that runoff-driven soil erosion in these alpine headwater streams is responsible for the export of ca. 0.3 to 0.8 gC m^{-2} a^{-1} as POC, which represents ca. 0.1 – 0.3 % of carbon fixed by NPP. Most of this soil OC export occurs during high-discharge events. Our study also shows that despite a significant variability in isotopic and molecular POC signatures at low discharge, all three catchments show a convergence of these signatures at higher discharges. Suspended sediment samples collected at above-average discharges are hence most representative of overall endmember contributions.

Plain Language Summary

Rivers are the "arteries" of the global organic carbon cycle as they allow for the transport of organic carbon between different reservoirs such as the biosphere, the hydrosphere, the atmosphere, and the geosphere. To better understand how organic carbon is harvested from landscapes, we use the geochemical signatures of particulate organic carbon transported in three small (<2 km) Swiss rivers to fingerprint its provenance. We are interested in how this provenance may change depending on the river discharge as this may bias typical estimates that rely on limited samples and may further reveal the mechanisms responsible for carbon mobilization. We find that at low discharges, the provenance of organic carbon in these catchments is highly variable. As runoff increases, the geochemical signatures of particulate organic carbon converge towards a well-defined endmember mixture. Overall, we also find that the contribution of soil-sourced organic carbon increases significantly with discharge and at a similar rate in all three catchments despite different landcover. This study suggests that rainfall and runoff are the main mechanisms of soil-derived carbon mobilization in these pre-alpine catchments.

1 Introduction

The erosion and riverine export of organic carbon from land to the ocean affects the global carbon cycle on a range of time-scales. The origin of the exported particulate organic carbon (POC) determines the impact of carbon transfer on global biogeochemical cycles: If biospheric carbon, i.e., carbon recently fixed by photosynthesis, is mobilized, transported, and eventually buried in oceanic sediment, the riverine export of carbon acts as an atmospheric carbon sink on geologic time-scales. However, the erosion, mobilization, and oxidation of petrogenic carbon, i.e., organic carbon contained in sedimentary rocks, constitutes a source of carbon to the atmosphere. The relative balance between biospheric carbon export and petrogenic carbon oxidation thus exerts a key control on the long-term carbon cycle and small changes in the balance between these two pathways have the potential to affect Earth's climate on geological time-scales (millions of years) (Berner, 1999; Hilton & West, 2020). On shorter time-scales of decades to millennia, mobilization of POC (and dissolved organic carbon) redistributes carbon between the Earth's surface reservoirs (Doetterl et al., 2016). Soils and vegetation contain more

than three times the amount of carbon held in the atmosphere (Jobbágy & Jackson, 2000). Perturbations of soil and vegetation systems have the potential to significantly affect the residence time of carbon in the biospheric reservoir (e.g., Berhe et al., 2007; Li et al., 2015; T. I. Eglinton et al., 2021) and the carbon budget of the atmosphere (Lal, 2004). Thus, to understand the significance of terrestrial POC mobilization for the global carbon cycle, not only the amount, but also the sources of exported POC need to be constrained.

The global export of POC from large fluvial catchments is primarily driven by physical erosion processes and is dominated by export from tectonically active areas (Stallard, 1998; Galy et al., 2015). However, climate - through its modulation of physical erosion processes - also contributes to the regulation of POC export (Hilton, 2017).). POC export fluxes have been observed to broadly scale with runoff (Smith et al., 2013; Clark et al., 2013, 2017; Goñi et al., 2013; Turowski et al., 2016; Hilton, 2017; Takagi & Haga, 2019; Wang et al., 2019; Baronas et al., 2020; Qiao et al., 2020; Qu et al., 2020). In some regions, this climatic regulation is further enhanced by extreme events such as storms that contribute disproportionally to POC export (Hilton et al., 2008; West et al., 2011). Climate and hydrology have also been suggested to impact the downstream preservation of organic matter in sedimentary basins as an invigorated hydrological cycle will promote rapid POC export, by-passing degradation processes upstream in the catchment (Yoshida et al., 2009; Leithold et al., 2006; Lee et al., 2019). Overall, these observations highlight a potential link between climate and surface carbon fluxes of global relevance. Nevertheless, most existing studies have focused on the modulation of total POC fluxes as a function of climate and river discharge, with only relatively few investigations addressing potential changes in specific carbon source associated with POC fluxes in the context of their contrasting influence on the long-term carbon cycle (Leithold et al., 2006; Blair et al., 2010; Galy & Eglinton, 2011; Hilton et al., 2012, 2015; Galy et al., 2015; Wang et al., 2019). To better understand mobilization mechanisms and short-term carbon cycle dynamics due to the redistribution of organic carbon between the Earth's surface reservoirs, a more detailed delineation of the sources of biospheric organic carbon in riverine sediments is necessary. In particular, attempts at identifying the response of terrestrial carbon pools to varying runoff conditions remain scarce. Those few studies undertaken thus far indicate that the chemical and isotopic composition of the exported carbon shifts towards signatures similar to topsoil at higher discharges (Smith et al., 2013; Clark et al., 2013; Goñi et al., 2013), implying a significant contribution of precipitation-driven erosion of plant litter and surface soil to overall organic carbon export fluxes. However, the extent to which such findings are germane to a broader range of catchments remains unclear.

In this study, we examine how variations in the runoff-driven erosion influence the contribution of different carbon source endmembers in three forested headwater catchments in the Swiss Prealps. To complement the current understanding of POC export in forested mountain catchments, we not only differentiate between petrogenic and biospheric carbon, but also constrain runoff-driven changes in the contributions of different endmembers, i.e., bedrock, soil and vegetation, based on a combined approach using both carbon isotopic and biomarker (n-alkane) signatures. Additionally, by comparing three similar small catchments in close proximity to one another and under the same climate conditions, we evaluate how well observations on the catchment-scale can be extrapolated to predict carbon export in similar settings.

2 Methods

The isotopic and chemical composition of POC allows tracing the contribution of different sources. Radiocarbon activity (expressed as $\Delta^{14}C$ or $F^{14}C$) is a powerful tool to differentiate between biospheric and petrogenic carbon sources, as the latter (fossil carbon) is devoid of ^{14}C. This isotopic contrast has often been used to quantify riverine export of biospheric POC (e.g., Leithold et al., 2006; Galy & Eglinton, 2011; Tao et

al., 2015; Wang et al., 2019). Here, we aim to further deconvolve contributions from different components of biospheric carbon, with topsoil, deeper soil and vegetation among the potential endmembers. Hence, in addition to the bulk isotopic composition of carbon, we also focus on the relative concentrations of long-chain (C_{25} - C_{33}), odd-carbon-numbered *n*-alkane biomarker lipids, that are constituents of plant leaf epicuticular waxes (G. Eglinton & Hamilton, 1967). These and other *n*-alkanes occur in all potential endmembers, including bedrock, soil and vegetation (Jansen & Wiesenberg, 2017), but with distinctive distributions in terms of *n*-alkane chain-length (e.g., Saliot et al., 1988; Zech et al., 2010; Schäfer et al., 2016), providing a diagnostic quantitative tracer of the sources of riverine POC.

2.1 Study site

The Erlenbach, Lümpenenbach and Vogelbach catchments are located within 5 km of each other in the Alptal valley in the Swiss Prealps (Figure 1). All three catchments have been in the focus of sustained hydrological research by the Swiss Federal Institute for Forest, Snow and Landscape (WSL) since 1967. Since 1985, discharge has been measured at 10-minute intervals at the catchment outlets. Annual precipitation in Alptal amounts to 2300 mm. The three streams are all roughly 2 km long with an average flow velocity around 5 m s^{-1} (Wyss et al., 2016). The average catchment elevation is 1300 m asl with an approximate elevation drop of 500 m for all three streams (FOEN, 2016), but they differ in area and landcover (Figure 1).

In each catchment, the forest consists mainly of Norway Spruce (*Picea abies*) and European Silver Fir (*Abies alba*) (Schleppi et al., 1998). The dominant soil type is a low-permeability clayey gleysol resulting in a ground water table close to the surface (Schleppi et al., 1998; Hagedorn et al., 2001). The Alptal is underlain by the Wägital-Flysch formation, a turbidite sequence of interbedded mudstones and sandstones of Eocene age (Winkler et al., 1985). The bedrock in the Erlenbach catchment is dominated by fine-grained impermeable material (Smith et al., 2013), where creep landslides deliver material from the hillslopes into the channels (Schuerch et al., 2006; Golly et al., 2017). This phenomenon is not observed in either Lümpenenbach or Vogelbach catchments (Molnar et al., 2010) where the bedrock is composed of calcareous sandstones (Milzow et al., 2006). POC export has been previously investigated in the Erlenbach by Smith et al. (2013). Based on carbon and nitrogen concentrations as well as stable isotopes, these authors attributed an observed increase of biospheric organic carbon at high discharges to mobilization by overland flow.

2.2 Sampling

Suspended sediment samples were collected in the course of two campaigns: First, Erlenbach (gauging station: 47.04501°, 8.70911°), Lümpenenbach (47.0465°, 8.705231°) and Vogelbach (47.07578°, 8.718217°) were sampled regularly once to twice per month between June 2014 and June 2015. Second, the rivers were sampled again between April and May 2016 on rainy days in order to target a range of above average discharges. Up to 40 L of water was collected at each site and passed through pre-combusted GF/F filters (mesh size 0.7 µm) within 24h of collection. To constrain potential endmembers that contribute carbon to the suspended sediment load, representative vegetation, topsoil, deeper soil, and bedrock samples were collected in the catchments. Bedrock and vegetation samples including the dominant tree species silver fir (*Abies alba*) and Norway spruce (*Picea abies*) as well as green alder (*Alnus viridis*), moss, three different grasses, common rush (*Juncus effusus*), horsetail (*equisetum*) and ground pines (*lycopodium*) were gathered in May 2015. 27 soil cores were collected in June 2016, as 3 groups of 9 cores each, two groups of grassland soils in the Lümpenenbach and Vogelbach catchment of 30 cm depth, one group of forest soils in the Vogelbach watershed limited to 10 cm depth as rocks in the subsurface impeded deeper sampling. Each group of cores was collected in a 3 x 3 pat-

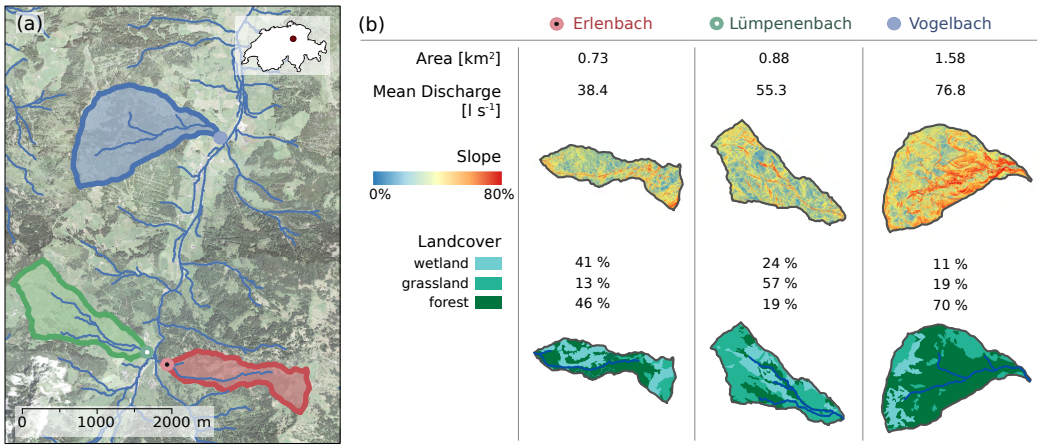

Figure 1. Overview of the three studied catchments. Information on area and mean discharge are provided by the WSL (WSL, 2020), slope and landcover maps are based on geodata ©swisstopo

tern in an area of 20 m^2 × 20 m^2. The cores were separated into "topsoil" and "deep soil" (<10 cm and >10 cm, respectively). In each case, 3 soil samples within the same group and depth interval were combined yielding in total 6 grassland top and deep soil samples, respectively, and 3 forest top soil samples. The soils and suspended sediment were analyzed for total organic carbon (TOC) content, $\delta^{13}C$, $\Delta^{14}C$ of bulk organic carbon, and long-chain n-alkane concentrations. For vegetation and bedrock samples, only n-alkanes were measured, as stable isotopes of these endmembers are reported in Smith et al. (2013), and $\Delta^{14}C$ values of vegetation are assumed to be equivalent to that of atmospheric carbon, while the Eocene age bedrock is considered radiocarbon dead.

2.3 Analytical procedures

For carbon isotope analysis, approximately 10 mg of soil or 30 to 35 mg of filter were transferred into silver boats (8 mm × 8 mm × 15 mm, Elemental Microanalysis) and left in a desiccator for fumigation at 60°C, first with 37 % hydrochloric acid to remove carbonates for four days, afterwards with NaOH pellets to neutralize the acid for another four days. The decarbonated samples were then wrapped in tin boats (8 mm × 8 mm × 15 mm, Elemental Microanalysis). Total organic carbon (TOC), $\delta^{13}C$ and $\Delta^{14}C$ are determined using the on-line EA-IRMS-AMS system operated by the Biogeoscience group in the Laboratory of Ion Beam Physics at ETH Zürich (McIntyre et al., 2017).

Lipids were extracted using a microwave accelerated reaction system (CEM MARS 5). Up to 55 mg of vegetation, between 5 and 10 g of soil, or a sediment-covered GF/F filter were transferred into teflon vessels and covered with a dichloromethane (DCM) : methanol (MeOH) 9:1 (v/v) solvent mixture. The extraction temperature was programmed to ramp to 100 °C in 35 min and was kept at this level for another 25 min. The resulting lipid extract was then dried under nitrogen flow and redissolved in 5 mL MilliQ water with NaCl. The neutral phase was back-extracted with hexane (Hex), from which the apolar fraction containing *n*-alkanes was separated on a 1 % deactivated silica column using Hex:DCM 9:1. Quantification of *n*-alkanes was performed on a GC-FID (gas chromatograph connected to a flame ionization detector, Agilent 7890A) using an external standard (Supelco Alkane standard solution C_{21} - C_{40}). Alkane concentrations are parametrized as carbon preference index (CPI), that increases with the amount of un-

even carbon numbers relative to even numbered n-alkanes (equation 1), adapted from Marzi et al. (1993)), and average chain length (ACL, equation 2, adapted from Poynter and Eglinton (1990)) , the weighted average of carbon chain lengths present in the sample (further information on alkane parametrization in the supplementary information).

$$CPI = \frac{1}{2}\left(\frac{\sum_{i=n}^{m} C_{2i+1}}{\sum_{i=n}^{m} C_{2i}}\right) + \frac{1}{2}\left(\frac{\sum_{i=n}^{m} C_{2i+1}}{\sum_{i=n+1}^{m+1} C_{2i}}\right) \; with \; n = 12 \; and \; m = 16 \tag{1}$$

$$ACL = \frac{\sum_{i=n}^{m} (2i+1) * C_{2i+1}}{\sum_{i=n}^{m} C_{2i+1}} \; with \; n = 12 \; and \; m = 16 \tag{2}$$

2.4 Inverse model

Several modelling approaches exist that are suitable to solve for the contribution of different endmembers to a mixture. For instance, the Bayesian MixSIAR framework (Stock et al., 2018) has been previously applied in river catchments to constrain endmember contributions (e.g., Brandt et al., 2016; Blake et al., 2018; Menges et al., 2020). In this study, the number of potential endmembers equals the number of measured parameters, and therefore a simple fully-determined system of linear equations is sufficient to delineate the contribution of different endmembers. This approach has previously been applied to riverine samples (e.g., Torres et al., 2016; Hemingway et al., 2020). As the streams are only about 2 km long and the average flow velocity is roughly 5 ms^{-1} (Wyss et al., 2016), transport times of suspended sediment are short and we therefore do not expect to observe transformations of the geochemical or isotopic signal of mobilised carbon during riverine transport. Working on the assumption that for each of the parameters investigated in this study (i.e., $\Delta^{14}C$, $\delta^{13}C$, CPI, ACL), the signal observed in the suspended sediment sample is the result of conservative mixing of the different endmembers, the suspended sediment sample can be modelled by a system of linear equations:

$$\begin{pmatrix} p_{1,1} & \cdots & p_{1,m} \\ \vdots & \ddots & \\ p_{n,1} & & p_{n,m} \\ 1 & \dots & 1 \end{pmatrix} \begin{pmatrix} x_1 \\ \vdots \\ x_m \end{pmatrix} = \begin{pmatrix} s_1 \\ \vdots \\ s_n \\ 1 \end{pmatrix} \tag{3}$$

where $p_{i,j}$ is the value of parameter i for endmember j, x_j is the fraction of carbon sourced from endmember j in the suspended sediment sample and s_i is the value of parameter i in the suspended sediment. The solution for x, the vector comprised by x_j, is additionally constrained, as all of the endmember proportions x_j need to be ≥ 0 and sum up to 1. Both s_i as well as a range of possible values for $p_{i,j}$ are measured. Based on these results the best fit for x_j is determined: For each of the potential endmembers, parameter values are picked randomly from a uniform distribution of one standard deviation around the mean parameter value determined for the respective endmember. The data is normalized using min-max feature scaling to restrict each of the parameters to values between 0 and 1. Then, the best fit for x and the root mean square error (RMSE) of the respective solution is obtained using the Python function 'scipy.optimize.nnls' (Virtanen et al., 2020). This procedure is repeated 10000 times. The 500 solutions with the smallest RMSE are used to calculate mean, median and mode of the potential solutions for x. If all metrics differ by less than 0.05 the distribution is not skewed and the mean is used to sum up the results, otherwise the median is chosen instead.

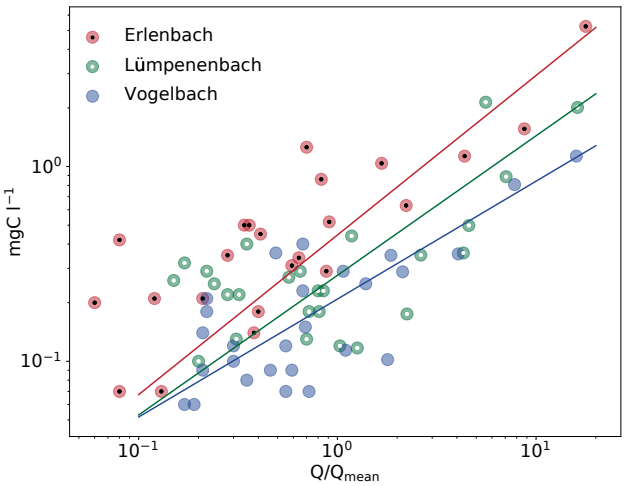

Figure 2. Carbon export increases at a similar rate in all three studied catchments. The fitted curves show power law relationships between Q/Q$_{mean}$ and exported carbon in mg l^{-1}

3 Results

3.1 Variations in carbon export with discharge

The overall export of organic carbon increases with discharge in all three catchments at a similar rate (Figure 2). To account for the different sizes of the catchments, discharge (Q) is reported relative to mean discharge (Q$_{mean}$) as Q/Q$_{mean}$. In all rivers, the exported carbon can be approximated using a power law ($a * x^b$) with exponents b of 0.82±0.09, 0.72±0.11 and 0.61±0.05 for the Erlenbach, Lümpenenbach, and Vogelbach, respectively. The exponent b for the Erlenbach determined in this study is lower compared to that (1.33) calculated in Smith (2013), but the highest of the three catchments.

The geochemical and isotopic parameters investigated in this study respond differently to changes in discharge (Figure 3. At low discharges, ^{14}C signatures exhibit large variability, with Δ^{14}C values ranging from less than -800 ‰ to more than -50 ‰. With increasing discharge, the radiocarbon signature appears to converge towards modern values ($\sim$ 50 ‰) in the Lümpenenbach and Vogelbach, while in the Erlenbach, Δ^{14}C signatures stabilize at significantly lower values (older ^{14}C ages), ca. -400 ‰, at high discharge. A Levene's test (Levene, 1961) shows that the difference in variance between samples collected at average or less than average discharge (Q/Q$_{mean}$ $\leq$ 1) and samples collected at higher-than-average discharges (Q/Q$_{mean}$ $\geq$ 1) is significant for the Erlenbach and the Vogelbach (p-value ¡ 0.05). Across all discharge levels, Δ^{14}C values in the Lümpenenenbach are less ^{14}C-depleted (mean Δ^{14}C, - 204 ± 164 ‰) compared to the other two catchments (Δ^{14}C of -362 ± 215 ‰ and -312 ± 250 ‰ for the Erlenbach and Vogelbach, respectively). Stable carbon isotopic (δ^{13}C) in any of the three catchments. Similarly, CPI does not correlate with discharge, but is significantly (p $\leq$ 0.01) higher in the Lümpenenbach catchment (CPI, 3 - 8) compared to the other rivers (CPI, 1 – 3). The ACL values are highly variable at Q/Q$_{mean}$ values < 1, while the variance decreases towards higher discharge.

PERMDISP (Anderson, 2006), a multivariate Levene's test, where all isotopic and alkane-based parameters are considered, reveals that the difference in measurement dispersion of samples collected at low discharges compared to samples taken at above-average discharges is significant at the 0.1-level in the Lümpenenbach, and the 0.05-level in the

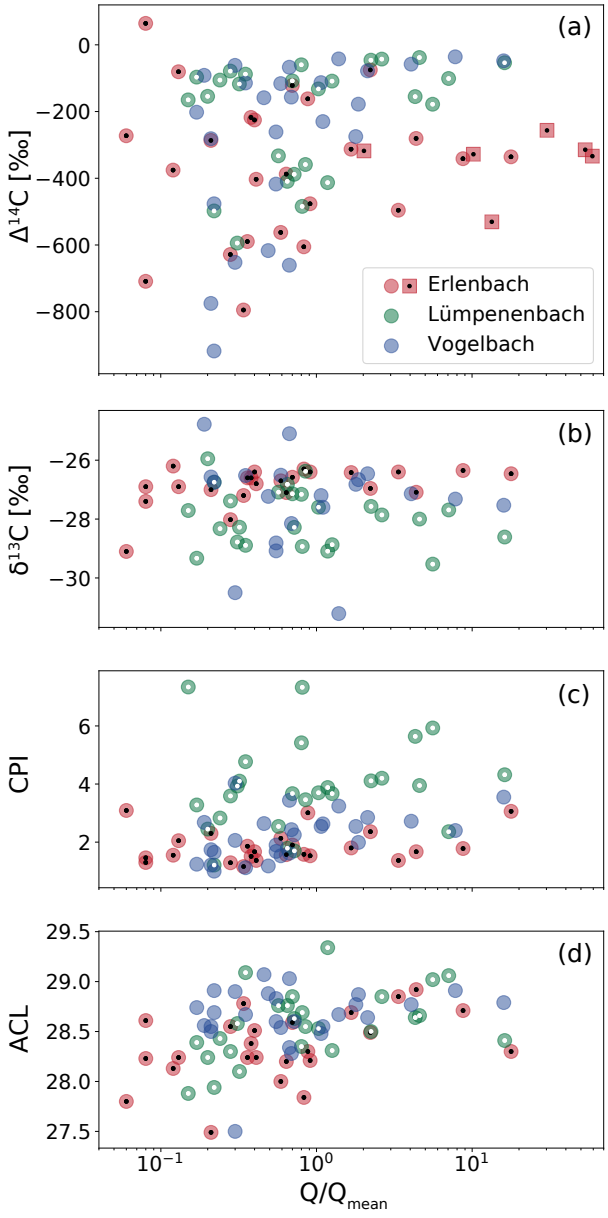

Figure 3. All investigated parameters as function of discharge Q/Q_{mean}. The squared Erlenbach symbols in panel a) represent $\Delta^{14}C$ data from Smith et al. (2013)

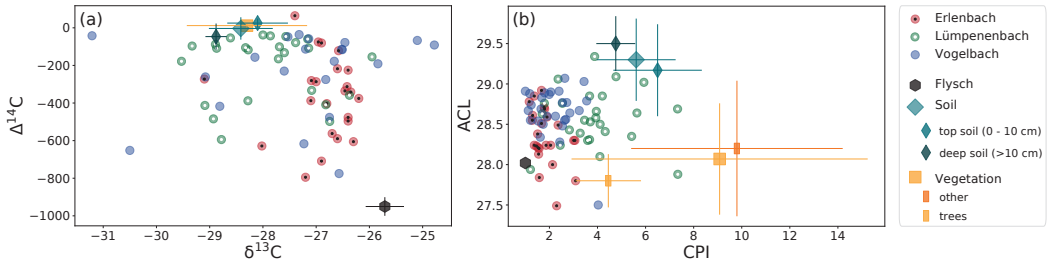

Figure 4. Delineating suspended sediment samples and potential sources of organic carbon using isotopes and *n*-alkanes. a) Using natural abundance $\delta^{13}C$ and $\Delta^{14}C$ does not allow a distinction of the different potential radiocarbon modern endmembers. b) Metrics based on *n*-alkanes make a distinction between soil- and vegetation-sourced endmembers possible.

Erlenbach and Vogelbach catchments, highlighting the role of the hydrological forcing in stabilizing POC chemical signatures.

3.2 Soil and suspended sediment samples in comparison to potential endmembers

The carbon isotopic signatures and *n*-alkane concentrations of topsoil and deep soil do not significantly differ between the catchments, or between forest and grassland soil. This confirms the observation by (Smith, 2013), where the investigated metrics did not differ between Erlenbach soils and Vogelbach soils. Thus, all topsoils and deep soils, respectively, are compiled, and the soil endmember is considered the same in all catchments. Both $\delta^{13}C$ and $\Delta^{14}C$ values are similar for the soil and vegetation endmembers (Figure 4). The $\delta^{13}C$ value of vegetation of -28.3 ± 1.1 (Smith et al., 2013) covers the entire range of stable carbon isotope compositions of organic carbon in topsoils (-28.1 ± 0.6) and deep soils (-28.9 ± 0.2). The endmembers also overlap in $\Delta^{14}C$ parameter space, with values of 11.9 ± 23.7 ‰, 25.2 ± 23.7 ‰ and -46.6 ± 69.4 ‰ for vegetation, topsoil and deep soil, respectively. These mean values are consistent with differences in turnover (Voort et al., 2019): i.e., while the $\Delta^{14}C$ values of vegetation are equivalent to modern atmospheric values, topsoil has a higher mean $\Delta^{14}C$ value due to an incorporation of bomb-derived ^{14}C that was introduced in the 1950s. Deep soil $\Delta^{14}C$ values are on average lower than vegetation and topsoil. Bedrock (Flysch) is assumed to be radiocarbon dead with 10% uncertainty, $\delta^{13}C$ is lower than in the modern endmembers (-25.7 ± 0.4 ‰, Smith et al. (2013)).

While the range of $\Delta^{14}C$ values for the suspended sediment samples is covered by the potential endmembers, the range of $\delta^{13}C$ values of the endmembers does not completely encompass the $\delta^{13}C$ variability observed for the suspended sediment samples, especially the Vogelbach samples ($\delta^{13}C$, -31.2 to -24.8 ‰)(Figure 4. The metrics based on *n*-alkanes overlap for deep soil (CPI: 4.8 ± 0.8, ACL: 29.5 ± 0.3) and top soil (CPI: 6.5 ± 1.8, ACL: 29.2 ± 0.6). In case of vegetation, the analyzed tree species (*Picea abies, Abies alba*) are well constrained with a CPI of 4.44 ± 1.4 and an ACL of 27.8 ± 0.3, while other vegetation samples (*Alnus viridis, Lycopodium, Equisetum, Juncus effusus*, grasses, moss) cover a large range of values (CPI: 9.8 ± 4.4, ACL: 28.2 ± 0.8). Further information on the *n*-alkane composition of the vegetation endmember is available in the supporting information. The CPI of Flysch has a value of 1 ± 0.2, markedly lower compared to soil and vegetation, while the ACL of Flysch is 28.0 ± 0.1. Many of the suspended sediment samples plot within the endmember values in the CPI - ACL - parameter space,

especially between flysch and soil (Figure 4b). Soils and flysch exhibit similar carbon-normalized concentrations of *n*-alkanes (169 ± 90 µg gOC^{-1} and 199 ± 41 µg gOC^{-1}, respectively), while *n*-alkane concentrations in plant tissue vary markedly among species, ranging from 66 µg gOC^{-1} for needles of silver fir (*Abies alba*) to 1227 µg gOC^{-1} in a grass sample.

4 Discussion

4.1 Constraints on endmember contributions using an inverse model

Carbon isotopes have been frequently used to determine sources of riverine carbon (e.g., Nagao et al., 2005; Hilton et al., 2008; Blair et al., 2010; Marwick et al., 2015; Tao et al., 2015; Wang et al., 2019; Menges et al., 2020) with radiocarbon particularly well suited to differentiate between modern biospheric carbon and radiocarbon-dead petrogenic carbon. Assuming riverine carbon can be modelled as a composite of bedrock containing a fixed proportion of fossil organic carbon and a modern endmember with an invariant radiocarbon signal, radiocarbon and TOC alone is sufficient to determine the contribution of each endmember. (Galy et al., 2008; Blair et al., 2010). If these assumptions hold true, $F^{14}C$ can then be described as a hyperbolic function of TOC with a curvature defined by the proportion of fossil carbon (Hemingway et al., 2018; Wang et al., 2019). As shown in Figure 5, a hyperbola is not found to be a suitable fit for the relation between %C and $F^{14}C$ in any of the catchments.

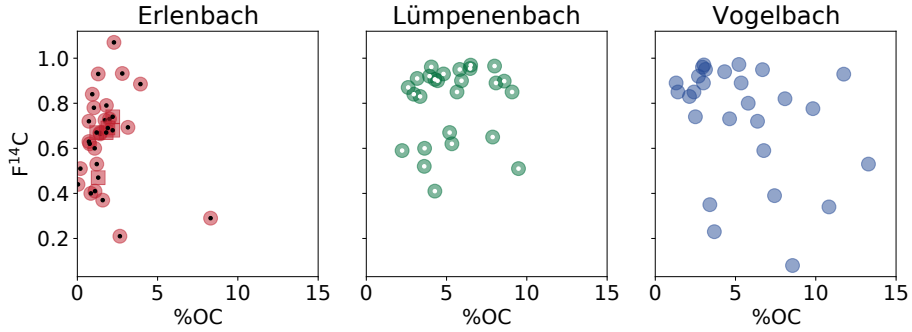

Figure 5. $F^{14}C$ as a function of organic carbon content in % If the observed radiocarbon signature in the catchments was explainable by mixing of two invariable endmembers, one of them radiocarbon modern, the other one radiocarbon dead, $F^{14}C$ would be a hyperbolic function of %C (Hemingway et al., 2018). Squared symbols in the Erlenbach plot display data from Smith et al. (2013)

The lack of such a relationship implies that either more than two endmembers are needed to explain the riverine organic carbon signal or that the TOC of the bedrock endmember is not invariant. The inverse model used in this study is not based on these requirements: the solution of the system of linear equations is the proportion of carbon in the sample derived from the respective endmembers and is hence independent of their TOC. The limit of endmembers that the model can solve for depends on the number of linear equations, and since four independent parameters were analyzed in this study, the model can solve for up to five endmembers.

While $\delta^{13}C$ and $\Delta^{14}C$ would be sufficient to solve for the contributions of up to 3 different endmembers, the potential sources of modern carbon, including the different types of soil and vegetation, are too similar to be resolved based on their carbon isotopic signatures alone (Figure 4) to allow a separation based on these characteristics alone.

The parameters based on long-chained *n*-alkanes, (i.e., CPI, ACL, Eq. 1 & 2), provide a further dimension to distinguish analyzed soil and vegetation samples, hence adding these metrics to the inversion model allows to constrain the contribution from different sources of biospheric organic carbon. An important consideration is whether the chosen parameters behave conservatively during transport and mixing. For example, ^{13}C fractionation has been observed during microbial respiration, soil development and sediment storage ([e.g., Mary et al., 1992; Schweizer et al., 1999; Fernandez et al., 2003; Werth & Kuzyakov, 2010; Scheingross et al., 2021). Furthermore, *n*-alkane based proxies may be affected by degradation (Buggle et al., 2010; Zech et al., 2010, 2012). However, as all rivers in this study are only 2 km long and devoid of significant sediment stores along their course, degradation effects occurring between the mobilization of organic carbon and sampling are considered negligible for modelling.

The parameters based on the relative abundances of different *n*-alkane homologues need to be weighted differently for each endmember if the concentrations of alkanes relative to TOC differ among the endmembers. As the flysch and the soil endmember are very similar in TOC-normalized *n*-alkane concentration 199 ± 41 µg gOC^{-1} and169 ± 90 µg gOC^{-1}, respectively) and the vegetation endmembers are difficult to constrain as they feature a variability of alkane concentrations (averaging all vegetation samples leads to 381 ± 355 µg gOC^{-1}), we assume similar alkane concentrations in all endmembers for simplicity, and therefore no weighting factor was applied.

As deep soil and top soil mostly overlap with respect the metrics used in this study, it is not possible to differentiate between organic carbon sourced from topsoil or deeper soil. Thus, the soil samples are combined to a single soil endmember (Figure 4). As the inverse model with 4 parameters can be solved for up to 5 endmembers, the dominant tree species in the catchment are considered separately from the other vegetation (further information in the appendix). Therefore, the model includes two different vegetation-derived endmembers, but their proportions are added subsequently to gain the overall contribution of vegetation-derived carbon. An additional potential endmember is POC derived from in-stream productivity. Given the short length of the streams and the average slope in the catchments ranges between 15 and 19% (FOEN, 2016), the residence time of water in the streams is short (Seeger & Weiler, 2014) and the potential impact of aquatic POC production hence expected to be insignificant, especially at higher discharges. It is therefore not included in the endmember analysis.

Figure 6, depicting the results of the inverse model, shows that suspended sediment samples from the Erlenbach catchment contain significantly higher proportions of Flysch than the sediments from the other rivers, as also reflected in the lower $\Delta^{14}C$ values in the Erlenbach samples (Figure 3(a)). The Lümpenenbach samples contain the least bedrock, with suspended sediment consisting of a maximum of 20% Flysch. This is consistent with the generally higher CPI and $\Delta^{14}C$ values for this catchment (Figure 3(a),(c)). The Vogelbach sediments cluster between the samples from the Erlenbach and the Lümpenenbach.

Figure 7 shows the proportion of each endmember as a function of discharge. In Lümpenenbach and Vogelbach, the fraction of flysch-derived carbon decreases with increasing discharge toward a value of less than 20% at $Q/Q_{mean} > 1$. In the Erlenbach, the contribution of petrogenic carbon is highly variable at low discharges and converges towards 40% with increasing discharge. This difference in proportion manifests itself in the export flux of flysch: While no significant trend with increasing discharge is observable in the Lümpenenbach and Vogelbach catchments, the flysch export in the Erlenbach increases significantly, leading to the offset in $\Delta^{14}C$ values of POC compared to the other catchments (Figure 3). In contrast, to petrogenic (flysch) carbon, the fraction of vegetation-derived organic carbon does not follow a specific trend with discharge, though proportions of vegetation that are $> 50\%$ are observed less often at $Q/Q_{mean} > 1$.

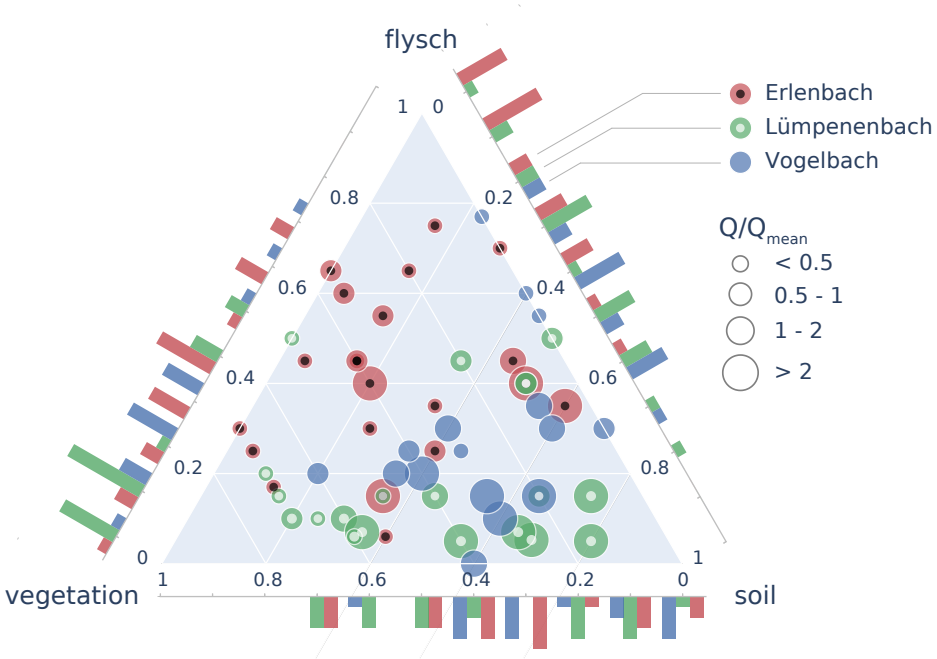

Figure 6. Ternary diagram displaying the fractions of flysch-, soil- and vegetation-derived carbon in the suspended sediment samples based on the inverse model The size of the markers corresponds to the discharge Q/Q_{mean} at sample collection. The histograms at each axis show the distribution of the respective endmember's carbon fractions in each river.

The proportion of soil-derived organic carbon increases with discharge in all three studied catchments., and the export flux of soil can be approximated in all catchments using a power law. The best fit yields similar values for exponent b (0.57±0.07 , 0.60± 0.2 and 0.7±0.08 for Erlenbach, Lümpenenbach and Vogelbach, respectively). The amount of carbon mobilized from soil is hence similar in all three catchments despite differences in landcover. Applying these rating functions to the discharge record for each of the Alptal streams (WSL, 2020) results in an annual erosion of soil organic carbon (SOC) of 0.7± 0.3 gSOC m^{-2} a^{-1}, 0.8 ± 0.4 gSOC m^{-2} a^{-1} and 0.3 ± 0.2 gSOC m^{-2} a^{-1} in the Erlenbach, Lümpenenbach and Vogelbach catchment, respectively. Organic carbon export linked to soil erosion hence accounts for roughly 0.1-0.3% of the net primary productivity of 445 gOC m^{-2} a^{-1} in the Alptal (Etzold et al., 2014). The modelled erosion of soil organic carbon in these pre-alpine catchments is an order of magnitude lower than the 9.6 m^{-2} a^{-1} estimated mean SOC exported by rivers from European croplands (Ciais et al., 2010). The results are therefore in accordance with the expectation that SOC erosion from the studied non-agricultural catchments are up to two orders of magnitude lower compared to croplands (Montgomery, 2007).

Runoff-driven mobilization of soil organic carbon has been suggested in a number of mountainous catchments (Hilton et al., 2008; Clark et al., 2013; Goñi et al., 2013; Hilton, 2017), including the Erlenbach (Smith et al., 2013). The results of the mixing model confirms that runoff exerts an important control on the export of soil organic carbon. The soil-sourced export increases with discharge at a similar rate in all three studied catchments, suggesting that estimates for mobilization of soil-derived organic carbon could potentially be extrapolated to other catchments in similar environmental settings.

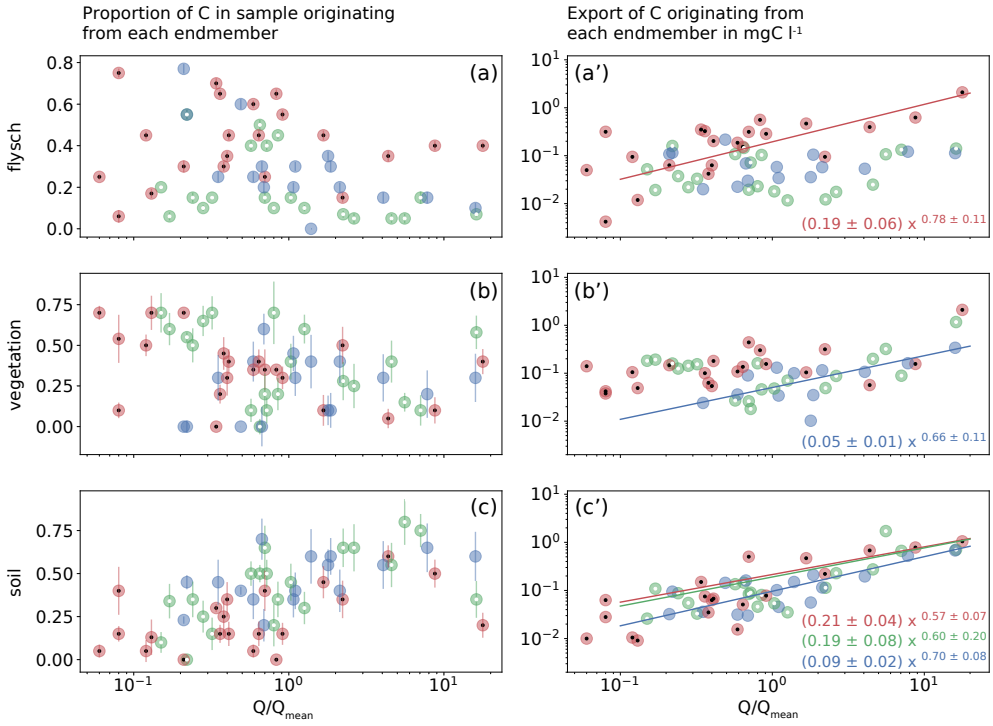

Figure 7. Export of organic carbon sourced from bedrock, vegetation and soil. The panels on the left show the proportion of suspended sediment organic carbon sourced from each endmember a) bedrock, b) vegetation and c) soil as a function of discharge. In the right column, the fluxes of each endmember are displayed. The fitted curves show powerlaw relationships between the exported carbon originating from the respective source and discharge Q/Q_{mean} that feature a value of $r^2 \geq 0.5$. The symbology is identical to the one used in Figure 2

In the Erlenbach catchment, organic carbon export during high discharge events has been monitored previously by Smith et al. (2013) with a resulting estimate of annual biospheric (vegetation- and soil-derived) carbon export of 14.0±4.4 gOC m^{-2} a^{-1}. Following the mixing model (Figure 6) the average proportion of soil organic carbon in biospheric carbon is $\sim$ 40% and even increases at higher discharges when most organic carbon is exported. This study's projection of 0.7 ± 0.3 gSOC m^{-2} a^{-1} in the Erlenbach does therefore not conform with the biospheric carbon export predicted by Smith et al. (2013). The difference in calculated export is caused by consistently lower organic carbon concentrations in the suspended sediment measured in this study (Supplementary Figure S4) compared to the data collected by Smith et al. (2013). This results in a lower exponent of the fitted power-law relating discharge and organic carbon export of 0.82±0.09 (Figure 2) compared to 1.33±0.08 (Smith et al., 2013). The differences in carbon concentration could be caused by different sampling strategies: While Smith et al. (2013) filtered 100ml water during storm events in July 2010, the suspended sediment samples analyzed in this study were collected between June 2014 and May 2016 by filtering 10 - 40 l of water. The different sample volumes could lead to inconsistencies between the different data sets. Additionally it is possible that carbon export fluxes are not constant and change over time. Carbon export may in the catchment may have fluctuated between 2010 and 2016. A seasonal shift is also possible, as the samples of Smith et al. (2013) were collected in July, while the suspended sediment in this study was sampled over the whole year, with most high discharge samples ($Q/Q_{mean} > 1$)

collected in April and May. The discrepancy between the data suggests that our estimate is comparatively conservative and constrains a lower boundary of soil-derived organic carbon export from forested mountainous headwater catchments.

In contrast with the two other catchments studied here, mobilization of petrogenic carbon in the Erlenbach is also enhanced with higher runoff . This additional mobilization of bedrock might be due to creep landslides that commonly occur in the Erlenbach catchment (Schuerch et al., 2006), but are not systematically observed in the two other catchments. These landslides are shallow failures of the unconsolidated glacial till that continuously deliver sediment into the channel (Schuerch et al., 2006; Golly et al., 2017). The impact of landslides in the Erlenbach catchment is also reflected in the order-of-magnitude higher overall sediment export in this catchment relative to the Lümpenenbach and Vogelbach (Figure 8). Geomorphic coupling between hillslope and channel and the resulting sediment yield thus impacts the balance of biospheric and petrogenic carbon export in forested mountainous catchments.

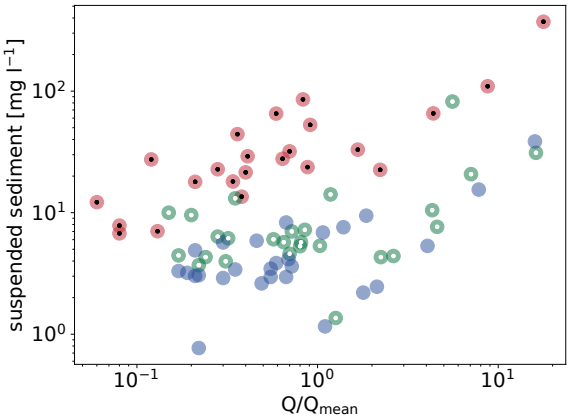

Figure 8. Fluxes of suspended sediment in each of the catchments as a function of discharge. The symbology is identical to the one used in Figure 2

4.2 Changes in organic matter characteristics with discharge

In all three headwater catchments, the variance of POC signatures decreases significantly with increasing discharge. As the isotopic and alkane-based parameters measured in the samples result from mixing of different endmembers, the observed convergence of parameter values implies that while at low discharges the contribution from the different sources varies considerably, carbon contributions from the respective sources at higher discharges are more uniform. The predominant sources at higher discharges vary between the studied catchments: In the Lümpenenbach and Vogelbach catchments, the results of the mixing model imply that only the export of carbon sourced from radiocarbon modern endmembers increases with discharge (Figure 7), leading to the observed stabilization at near modern $\Delta^{14}C$ values. In contrast, export of flysch-derived carbon increases along with soil-sourced carbon in the Erlenbach, and hence $\Delta^{14}C$ values converge at intermediate values (-300 to -400‰), reflecting a mixture of petrogenic and modern carbon.

Increasing uniformity in the chemical or isotopic composition of riverine POC at high discharges has been observed previously in some mountainous catchments, with the sample composition converging towards carbon predominantly sourced from bedrock in

the Waipaoa river (Gomez et al., 2003) or soil in the Jiolong river (Qiao et al., 2020). Takagi and Haga (2019) show a distinct convergence of C/N in suspended sediment samples with discharge in a Japanese headwater catchment. In contrast, almost no reduction in geochemical variability has been observed in the Santa Clara, Umpqua and Eel rivers (Hatten et al., 2012; Goñi et al., 2013), while in the Min Jiang river (Wang et al., 2019), the variance in $\delta^{13}C$ values decreases significantly only at one of the six sampling locations (Heishui station). Currently, however, studies that focus on changes of the composition of POC with discharge and encompass a sample density that is sufficiently high to constrain differences in variance remain too sparse to constrain those conditions that drive convergence of POC composition, and to determine the isotopic or chemical compositions upon which POC will converge with increasing discharge. Putatively, the convergence occurs due to the availability of carbon from different sources at low compared to high discharges. At low discharges, a river may mostly mobilize carbon available within or in close proximity to the channel. In case of the studied mountainous rivers, several sources of carbon with distinct isotopic and geochemical are available at or close to the channel including the incised bedrock, soil of different depths and vegetation. During high-discharge events, carbon eroded from the hillslopes by runoff seems to dominate the exported POC, therefore the composition of POC may converge towards the carbon available for runoff-driven surface erosion in the respective catchment. Further studies targeting this question would improve our understanding of the processes that drive the balance between biospheric and petrogenic organic carbon export, as well as our ability to predict and refine riverine organic carbon export fluxes from small mountainous catchments.

The observed decrease in chemical and isotopic variability within suspended sediment POC with increasing discharge implies that suspended samples should ideally be collected at above-average discharges in order to best approximate the overall carbon export. Additionally, high discharge events contribute disproportionally to the overall carbon flux, thus the endmember contributions observed during these conditions have higher relevance for the overall carbon export. In contrast, samples collected during low flow conditions may not be representative given that the contribution of different carbon sources may shift with increasing discharge, and that intrinsic sample-to-sample variability is likely to be higher.

5 Conclusions

We applied an inverse model using bulk carbon isotopes and *n*-alkane metrics (i.e., CPI and ACL) to suspended sediment samples from three pre-alpine headwater catchments to assess the fractional contribution of putative sources of organic carbon, namely bedrock, soil, and vegetation. The results of the model reveal an increase of soil-sourced organic carbon with discharge due to runoff-driven erosion across all three studied catchments. This indicates that the export fluxes of soil organic carbon can potentially be extrapolated to other temperate mountain catchments despite contrasting bulk POC signatures. Differences in the exported carbon signal among the three studied catchments manifest themselves most strongly in radiocarbon signatures, with significantly lower $\Delta^{14}C$ values at high discharge in the Erlenbach compared to the other two catchments. This offset is due to an enhanced export of petrogenic carbon at high discharge that is only observed in the Erlenbach catchment, and likely reflects landslides that mobilized bedrock-sourced sediment. Notably, all three catchments show a convergence in chemical and isotopic compositions at higher discharges. Suspended sediment samples collected at above-average discharges are thus better suited to constrain carbon export since their composition is most representative of overall end-member contributions.

Acknowledgments

The data set and script of the mixing model used in this study is available at https://doi.org/10.3929/ethz-b-000502657

This study was funded by the Swiss National Science Foundation ("CAPS-LOCK2"&"CAPS-LOCK3"; #184865)

We thank Hermann Blum, Sebastian Brünecke, Elena Leisibach and Andrea Winter for their help with sampling and Christine Alewell and Frank Hagedorn for the helpful discussions. We thank the Laboratory for Ion Beam Physics (ETH) for their support with the Accelerator Mass Spectrometry measurements.

The authors declare that they have no competing interests.

References

Anderson, M. J. (2006). Distance-based tests for homogeneity of multivariate dispersions. *Biometrics*, *62*(1), 245–253.

Baronas, J. J., Stevenson, E. I., Hackney, C. R., Darby, S. E., Bickle, M. J., Hilton, R. G., ... Tipper, E. T. (2020). Integrating suspended sediment flux in large alluvial river channels: Application of a synoptic rouse-based model to the irrawaddy and salween rivers. *Journal of Geophysical Research: Earth Surface*, *125*(9), e2020JF005554.

Berhe, A. A., Harte, J., Harden, J. W., & Torn, M. S. (2007). The significance of the erosion-induced terrestrial carbon sink. *BioScience*, *57*(4), 337–346.

Berner, R. A. (1999). A new look at the long-term carbon cycle. *GSA Today*, *9*(11), 1–6.

Blair, N. E., Leithold, E., Brackley, H., Trustrum, N., Page, M., & Childress, L. (2010). Terrestrial sources and export of particulate organic carbon in the waipaoa sedimentary system: Problems, progress and processes. *Marine Geology*, *270*(1-4), 108–118.

Blake, W. H., Boeckx, P., Stock, B. C., Smith, H. G., Bodé, S., Upadhayay, H. R., ... others (2018). A deconvolutional bayesian mixing model approach for river basin sediment source apportionment. *Scientific reports*, *8*(1), 1–12.

Brandt, C., Cadisch, G., Nguyen, L. T., Vien, T. D., & Rasche, F. (2016). Compound-specific δ13c isotopes and bayesian inference for erosion estimates under different land use in vietnam. *Geoderma Regional*, *7*(3), 311–322.

Buggle, B., Wiesenberg, G. L., & Glaser, B. (2010). Is there a possibility to correct fossil n-alkane data for postsedimentary alteration effects? *Applied Geochemistry*, *25*(7), 947–957.

Ciais, P., Wattenbach, M., Vuichard, N., Smith, P., Piao, S., Don, A., ... others (2010). The european carbon balance. part 2: croplands. *Global Change Biology*, *16*(5), 1409–1428.

Clark, K., Hilton, R., West, A., Malhi, Y., Gröcke, D., Bryant, C., ... New, M. (2013). New views on "old" carbon in the amazon river: Insight from the source of organic carbon eroded from the peruvian andes. *Geochemistry, Geophysics, Geosystems*, *14*(5), 1644–1659.

Clark, K., Hilton, R., West, A., Robles Caceres, A., Gröcke, D., Marthews, T., ... Malhi, Y. (2017). Erosion of organic carbon from the andes and its effects on ecosystem carbon dioxide balance. *Journal of Geophysical Research: Biogeosciences*, *122*(3), 449–469.

Doetterl, S., Berhe, A. A., Nadeu, E., Wang, Z., Sommer, M., & Fiener, P. (2016). Erosion, deposition and soil carbon: A review of process-level controls, experimental tools and models to address c cycling in dynamic landscapes. *Earth-Science Reviews*, *154*, 102–122.

Eglinton, G., & Hamilton, R. J. (1967). Leaf epicuticular waxes. *Science*, *156*(3780), 1322–1335.

Eglinton, T. I., Galy, V. V., Hemingway, J. D., Feng, X., Bao, H., Blattmann, T. M., ... Zhao, M. (2021). Climate control on terrestrial biospheric carbon turnover. *Proceedings of the National Academy of Sciences*, *118*(8).

Etzold, S., Waldner, P., Thimonier, A., Schmitt, M., & Dobbertin, M. (2014). Tree growth in swiss forests between 1995 and 2010 in relation to climate and stand conditions: Recent disturbances matter. *Forest Ecology and Management*, *311*, 41–55.

Fernandez, I., Mahieu, N., & Cadisch, G. (2003). Carbon isotopic fractionation during decomposition of plant materials of different quality. *Global biogeochemical cycles*, *17*(3).

FOEN, Federal Office of the Environment. (2016). *Beschreibungen der naduf - messstandorte.* `https://www.bafu.admin.ch/bafu/en/home/topics/water/state/water--monitoring-networks.html`. (Accessed: 11.10.2020)

Galy, V., Beyssac, O., France-Lanord, C., & Eglinton, T. (2008). Recycling of graphite during himalayan erosion: a geological stabilization of carbon in the crust. *Science*, *322*(5903), 943–945.

Galy, V., & Eglinton, T. (2011). Protracted storage of biospheric carbon in the ganges–brahmaputra basin. *Nature Geoscience*, *4*(12), 843–847.

Galy, V., Peucker-Ehrenbrink, B., & Eglinton, T. (2015). Global carbon export from the terrestrial biosphere controlled by erosion. *Nature*, *521*(7551), 204–207.

Golly, A., Turowski, J. M., Badoux, A., & Hovius, N. (2017). Controls and feedbacks in the coupling of mountain channels and hillslopes. *Geology*, *45*(4), 307–310.

Gomez, B., Trustrum, N., Hicks, D., Rogers, K., Page, M., & Tate, K. (2003). Production, storage, and output of particulate organic carbon: Waipaoa river basin, new zealand. *Water Resources Research*, *39*(6).

Goñi, M. A., Hatten, J. A., Wheatcroft, R. A., & Borgeld, J. C. (2013). Particulate organic matter export by two contrasting small mountainous rivers from the pacific northwest, usa. *Journal of Geophysical Research: Biogeosciences*, *118*(1), 112–134.

Hagedorn, F., Bucher, J. B., & Schleppi, P. (2001). Contrasting dynamics of dissolved inorganic and organic nitrogen in soil and surface waters of forested catchments with gleysols. *Geoderma*, *100*(1-2), 173–192.

Hatten, J. A., Goñi, M. A., & Wheatcroft, R. A. (2012). Chemical characteristics of particulate organic matter from a small, mountainous river system in the oregon coast range, usa. *Biogeochemistry*, *107*(1-3), 43–66.

Hemingway, J. D., Hilton, R. G., Hovius, N., Eglinton, T. I., Haghipour, N., Wacker, L., ... Galy, V. V. (2018). Microbial oxidation of lithospheric organic carbon in rapidly eroding tropical mountain soils. *Science*, *360*(6385), 209–212.

Hemingway, J. D., Olson, H., Turchyn, A. V., Tipper, E. T., Bickle, M. J., & Johnston, D. T. (2020). Triple oxygen isotope insight into terrestrial pyrite oxidation. *Proceedings of the National Academy of Sciences*, *117*(14), 7650–7657.

Hilton, R. G. (2017). Climate regulates the erosional carbon export from the terrestrial biosphere. *Geomorphology*, *277*, 118–132.

Hilton, R. G., Galy, A., Hovius, N., Chen, M.-C., Horng, M.-J., & Chen, H. (2008). Tropical-cyclone-driven erosion of the terrestrial biosphere from mountains. *Nature Geoscience*, *1*(11), 759–762.

Hilton, R. G., Galy, A., Hovius, N., Kao, S.-J., Horng, M.-J., & Chen, H. (2012). Climatic and geomorphic controls on the erosion of terrestrial biomass from subtropical mountain forest. *Global Biogeochemical Cycles*, *26*(3).

Hilton, R. G., Galy, V., Gaillardet, J., Dellinger, M., Bryant, C., O'Regan, M., ... Calmels, D. (2015). Erosion of organic carbon in the arctic as a geological carbon dioxide sink. *Nature*, *524*(7563), 84–87.

Hilton, R. G., & West, A. J. (2020). Mountains, erosion and the carbon cycle. *Nature Reviews Earth & Environment*, *1*(6), 284–299.

Jansen, B., & Wiesenberg, G. L. (2017). Opportunities and limitations related to the application of plant-derived lipid molecular proxies in soil science. *Soil*, *3*(4), 211–234.

Jobbágy, E. G., & Jackson, R. B. (2000). The vertical distribution of soil organic carbon and its relation to climate and vegetation. *Ecological applications*, *10*(2), 423–436.

Lal, R. (2004). Soil carbon sequestration impacts on global climate change and food security. *science*, *304*(5677), 1623–1627.

Lee, H., Galy, V., Feng, X., Ponton, C., Galy, A., France-Lanord, C., & Feakins, S. J. (2019). Sustained wood burial in the bengal fan over the last 19 my. *Proceedings of the National Academy of Sciences*, *116*(45), 22518–22525.

Leithold, E. L., Blair, N. E., & Perkey, D. W. (2006). Geomorphologic controls on the age of particulate organic carbon from small mountainous and upland rivers. *Global Biogeochemical Cycles*, *20*(3).

Levene, H. (1961). Robust tests for equality of variances. *Contributions to probability and statistics. Essays in honor of Harold Hotelling*, 279–292.

Li, Y., Quine, T., Yu, H., Govers, G., Six, J., Gong, D., ... Van Oost, K. (2015). Sustained high magnitude erosional forcing generates an organic carbon sink: Test and implications in the loess plateau, china. *Earth and Planetary Science Letters*, *411*, 281–289.

Marwick, T. R., Tamooh, F., Teodoru, C. R., Borges, A. V., Darchambeau, F., & Bouillon, S. (2015). The age of river-transported carbon: A global perspective. *Global Biogeochemical Cycles*, *29*(2), 122–137.

Mary, B., Mariotti, A., & Morel, J. (1992). Use ofr 13c variations at natural abundance for studying the biodegradation of root mucilage, roots and glucose in soil. *Soil Biology and Biochemistry*, *24*(10), 1065–1072.

Marzi, R., Torkelson, B., & Olson, R. (1993). A revised carbon preference index. *Organic Geochemistry*, *20*(8), 1303–1306.

McIntyre, C. P., Wacker, L., Haghipour, N., Blattmann, T. M., Fahrni, S., Usman, M., ... Synal, H.-A. (2017). Online 13 c and 14 c gas measurements by ea-irms–ams at eth zürich. *Radiocarbon*, *59*(3), 893–903.

Menges, J., Hovius, N., Andermann, C., Lupker, M., Haghipour, N., Märki, L., & Sachse, D. (2020). Variations in organic carbon sourcing along a trans-himalayan river determined by a bayesian mixing approach. *Geochimica et Cosmochimica Acta*, *286*, 159–176.

Milzow, C., Molnar, P., McArdell, B. W., & Burlando, P. (2006). Spatial organization in the step-pool structure of a steep mountain stream (vogelbach, switzerland). *Water Resources Research*, *42*(4).

Molnar, P., Densmore, A. L., McArdell, B. W., Turowski, J. M., & Burlando, P. (2010). Analysis of changes in the step-pool morphology and channel profile of a steep mountain stream following a large flood. *Geomorphology*, *124*(1-2), 85–94.

Montgomery, D. R. (2007). Soil erosion and agricultural sustainability. *Proceedings of the National Academy of Sciences*, *104*(33), 13268–13272.

Nagao, S., Usui, T., Yamamoto, M., Minagawa, M., Iwatsuki, T., & Noda, A. (2005). Combined use of δ14c and δ13c values to trace transportation and deposition processes of terrestrial particulate organic matter in coastal marine environments. *Chemical Geology*, *218*(1-2), 63–72.

Poynter, J., & Eglinton, G. (1990). 14. molecular composition of three sediments from hole 717c: The bengal fan. In *Proceedings of the ocean drilling program: Scientific results* (Vol. 116, pp. 155–161).

Qiao, J., Bao, H., Huang, D., Li, D.-W., Lee, T.-Y., Huang, J.-C., & Kao, S.-J. (2020). Runoff-driven export of terrigenous particulate organic matter from

a small mountainous river: sources, fluxes and comparisons among different rivers. *Biogeochemistry*, *147*(1), 71–86.

Qu, Y., Jin, Z., Wang, J., Wang, Y., Xiao, J., Gou, L.-F., ... others (2020). The sources and seasonal fluxes of particulate organic carbon in the yellow river. *Earth Surface Processes and Landforms*.

Saliot, A., Tronczynski, J., Scribe, P., & Letolle, R. (1988). The application of isotopic and biogeochemical markers to the study of the biochemistry of organic matter in a macrotidal estuary, the loire, france. *Estuarine, Coastal and Shelf Science*, *27*(6), 645–669.

Schäfer, I. K., Lanny, V., Franke, J., Eglinton, T. I., Zech, M., Vysloužilová, B., & Zech, R. (2016). Leaf waxes in litter and topsoils along a european transect. *Soil*, *2*(4), 551–564.

Scheingross, J. S., Repasch, M. N., Hovius, N., Sachse, D., Lupker, M., Fuchs, M., ... others (2021). The fate of fluvially-deposited organic carbon during transient floodplain storage. *Earth and Planetary Science Letters*, *561*, 116822.

Schleppi, P., Muller, N., Feyen, H., Papritz, A., Bucher, J. B., & Flühler, H. (1998). Nitrogen budgets of two small experimental forested catchments at alptal, switzerland. *Forest Ecology and Management*, *101*(1-3), 177–185.

Schuerch, P., Densmore, A. L., McArdell, B. W., & Molnar, P. (2006). The influence of landsliding on sediment supply and channel change in a steep mountain catchment. *Geomorphology*, *78*(3-4), 222–235.

Schweizer, M., Fear, J., & Cadisch, G. (1999). Isotopic (13c) fractionation during plant residue decomposition and its implications for soil organic matter studies. *Rapid Communications in Mass Spectrometry*, *13*(13), 1284–1290.

Seeger, S., & Weiler, M. (2014). Reevaluation of transit time distributions, mean transit times and their relation to catchment topography. *Hydrology and Earth System Sciences*, *18*(12), 4751–4771.

Smith, J. C. (2013). *Particulate organic carbon mobilisation and export from temperate forested uplands* (Unpublished doctoral dissertation). University of Cambridge.

Smith, J. C., Galy, A., Hovius, N., Tye, A. M., Turowski, J. M., & Schleppi, P. (2013). Runoff-driven export of particulate organic carbon from soil in temperate forested uplands. *Earth and Planetary Science Letters*, *365*, 198–208.

Stallard, R. F. (1998). Terrestrial sedimentation and the carbon cycle: Coupling weathering and erosion to carbon burial. *Global Biogeochemical Cycles*, *12*(2), 231–257.

Stock, B. C., Jackson, A. L., Ward, E. J., Parnell, A. C., Phillips, D. L., & Semmens, B. X. (2018). Analyzing mixing systems using a new generation of bayesian tracer mixing models. *PeerJ*, *6*, e5096.

Takagi, M., & Haga, H. (2019). Carbon and nitrogen exports from forested headwater catchment in southwestern japan. *Biogeochemistry*, *145*(1-2), 35–46.

Tao, S., Eglinton, T. I., Montluçon, D. B., McIntyre, C., & Zhao, M. (2015). Pre-aged soil organic carbon as a major component of the yellow river suspended load: Regional significance and global relevance. *Earth and Planetary Science Letters*, *414*, 77–86.

Torres, M. A., West, A. J., Clark, K. E., Paris, G., Bouchez, J., Ponton, C., ... Adkins, J. F. (2016). The acid and alkalinity budgets of weathering in the andes–amazon system: Insights into the erosional control of global biogeochemical cycles. *Earth and Planetary Science Letters*, *450*, 381–391.

Turowski, J. M., Hilton, R. G., & Sparkes, R. (2016). Decadal carbon discharge by a mountain stream is dominated by coarse organic matter. *Geology*, *44*(1), 27–30.

Virtanen, P., Gommers, R., Oliphant, T. E., Haberland, M., Reddy, T., Cournapeau, D., ... SciPy 1.0 Contributors (2020). SciPy 1.0: Fundamental Algorithms for Scientific Computing in Python. *Nature Methods*, *17*, 261–272. doi:

10.1038/s41592-019-0686-2

Voort, T. S. v. d., Mannu, U., Hagedorn, F., McIntyre, C., Walthert, L., Schleppi, P., ... Eglinton, T. I. (2019). Dynamics of deep soil carbon–insights from 14 c time series across a climatic gradient. *Biogeosciences*, *16*(16), 3233–3246.

Wang, J., Hilton, R. G., Jin, Z., Zhang, F., Densmore, A. L., Gröcke, D. R., ... West, A. J. (2019). The isotopic composition and fluxes of particulate organic carbon exported from the eastern margin of the tibetan plateau. *Geochimica et Cosmochimica Acta*, *252*, 1–15.

Werth, M., & Kuzyakov, Y. (2010). 13c fractionation at the root–microorganisms–soil interface: a review and outlook for partitioning studies. *Soil Biology and Biochemistry*, *42*(9), 1372–1384.

West, A., Lin, C.-W., Lin, T.-C., Hilton, R., Liu, S.-H., Chang, C.-T., ... Hovius, N. (2011). Mobilization and transport of coarse woody debris to the oceans triggered by an extreme tropical storm. *Limnology and oceanography*, *56*(1), 77–85.

Winkler, W., Galetti, G., & Maggetti, M. (1985). Bentonite im gurnigel-, schlieren- und wägital flysch: Mineralogie, chemismus, herkunft. *Eclogae Geologicae Helvetiae*, *78*(3), 545–564.

WSL, Eidg. Forschungsanstalt für Wald, Schnee und Landschaft. (2020). *Wildbachforschung im alptal - untersuchungsgebiet.* `https://www.wsl.ch/de/ueber-die-wsl/versuchsanlagen-und-labors/naturgefahren-anlagen/wildbachforschung-im-alptal/untersuchungsgebiet.html`. (Accessed: 11.10.2020)

Wyss, C. R., Rickenmann, D., Fritschi, B., Turowski, J. M., Weitbrecht, V., & Boes, R. M. (2016). Measuring bed load transport rates by grain-size fraction using the swiss plate geophone signal at the erlenbach. *Journal of Hydraulic Engineering*, *142*(5), 04016003.

Yoshida, M., Yoshiuchi, Y., & Hoyanagi, K. (2009). Occurrence conditions of hyperpycnal flows, and their significance for organic-matter sedimentation in a holocene estuary, niigata plain, central japan. *Island Arc*, *18*(2), 320–332.

Zech, M., Buggle, B., Leiber, K., Marković, S., Glaser, B., Hambach, U., ... others (2010). Reconstructing quaternary vegetation history in the carpathian basin, se-europe, using n-alkane biomarkers as molecular fossils: Problems and possible solutions, potential and limitations. *E&G Quaternary Science Journal*, *58*(2), 148–155.

Zech, M., Rass, S., Buggle, B., Löscher, M., & Zöller, L. (2012). Reconstruction of the late quaternary paleoenvironments of the nussloch loess paleosol sequence, germany, using n-alkane biomarkers. *Quaternary Research*, *78*(2), 226–235.